European Journal of Mechanics / A Solids 100 (2023) 105029

Contents lists available at ScienceDirect

European Journal of Mechanics / A Solids

journal homepage: www.elsevier.com/locate/ejmsol

Size-dependent thermal bending of bilayer microbeam based on modified couple stress theory and Timoshenko beam theory

Xuan Ye [a,b], Hansong Ma [b], Xiaoming Liu [b,c,*], Yueguang Wei [d]

[a] Institute of Nuclear and New Energy Technology, Tsinghua University, Beijing, 100084, China
[b] LNM Institute of Mechanics, Chinese Academy of Sciences, Beijing, 100190, China
[c] School of Engineering Science, UCAS, Beijing, 100049, China
[d] College of Engineering, Peking University, Beijing, 100871, China

ARTICLE INFO

Keywords:
Bilayer beam
Thermal actuation
Size and shear effect
Modified couple stress theory

ABSTRACT

The bilayer microbeam can be assigned with two different thermal expansion coefficients, so that the microbeam can be used as a thermal actuator, which can provide bending with thermal loading. As a microdevice, the size effect plays an important role. In addition, the length height ratio L/h of the microbeam has to be smaller than 20, to provide sufficient support. With this ratio, the shear effect of the beam can not be ignored. In this work, considering both the size and shear effects, we modified the couple stress and Timoshenko beam theories to study the thermal bending of bilayer microbeams. By using the principle of minimum potential energy, we derived the higher-order governing equations under thermal load. Then with specified boundary conditions, we adopted the differential quadrature method to solve the governing equations. Finally, using a bilayer microbeam made of aluminum and polysilicon as an example, we verified effects of transverse shear and beam size. Results show that the size effect on beam stiffness is significant when the beam height is on the order of equivalent length scale (l_{eq}). Moreover, considering the transverse shear effect indicates that the lateral deflection of the Timoshenko beam depends on the ratio L/h: as L/h increases, the tip deflection increases and converges to the classical solution. Specifically, for a Timoshenko beam with $h/l_{eq} = 15$, the change in deflection can reach 44.6% when L/h is increased from 5 to 25.

1. Introduction

Due to high efficiency and compact integration, micro-/nanobeams have been widely used in semiconducting capacitors (Cheng et al., 2013), thermal/electrical sensors, and actuators (Wang et al., 2016; LeeladharRaturi et al., 2017; Cheng and Hu, 2021). With a quick response, we can apply thermal loading (Wang et al., 2020) to control these advanced devices. Single microbeams (Sellinger et al., 2010) have been widely used as key components of thermal actuators. Moreover, bilayer beams (Chen et al., 2011a; Sachyani et al., 2017) have been assembled as thermal actuators to achieve unique motions. In other words, the bilayer beam can control the motion of the thermal actuator more accurately and efficiently. Meanwhile, the nonlinear vibration behavior of microscale and marcoscale bilayer structures has also attracted the attention of researchers. Hao et al. (Hao and Ke, 2022; Hao et al., 2023) proposed analytical models for bilayer beams and unsymmetric double-layer lattice truss core sandwich beams, and found some interesting phenomenons of softening-spring nonlinearity due to the bending-extension coupling effect. For micro-scale bilayer beams and structures, it is necessary to consider the following factors: geometries, mechanical/thermal properties, and microstructures.

Length/height ratio (L/h) is an important geometric parameter in the micro-beam system, because for a short beam with a small value of L/h, the shear effect of the beam can be enormous. As stated in the references (Wang, 2013; Kim et al., 2016), the shear effect can not be ignored when the length/height ratio (L/h) is less than 20. For instance, Salvetat's bending experiment shows that the shear effect on single-walled carbon nanotube rope becomes important when the length/radius ratio is small (Salvetat et al., 1999). Wang's simulation results indicated that the effects of shear deformation and rotary inertia need to be considered for predicting the performance of short piezoelectric beams ($L/h < 20$) (Wang, 2013). In the micro-electromechanical systems (MEMS), many short micro-/nanoscale beams are designed within smaller ratios L/h to provide high stiffness, for example as motion stages (Kim et al., 2016;

* Corresponding author. LNM Institute of Mechanics, Chinese Academy of Sciences, Beijing, 100190, China.
E-mail address: xiaomingliu@imech.ac.cn (X. Liu).

https://doi.org/10.1016/j.euromechsol.2023.105029
Received 13 January 2023; Received in revised form 9 April 2023; Accepted 7 May 2023
Available online 8 May 2023

Potekhina and Wang, 2019). On another hand, an important factor affecting the deformation behavior of micro-/nanoscale beams is the size effect. The size effect can not be ignored (Stölken and Evans, 1998; Lam et al., 2003) as the beam approaches the size of the material's microstructure, which is usually on the order of microns or sub-microns. Ignoring the size effect, we may not only underestimate static stiffness (Akgöz and Civalek, 2013) and buckling load (Akgöz and Civalek, 2011), but also misinterpret nonlinear resonance frequencies and maximum amplitude (Dai et al., 2015). The size effect can not be explained by classical elastic beam theory due to the lack of material length scale parameters; while the intrinsic length parameters can be taken into account by higher-order theoretical models such as the strain gradient family, microcontinuum, and nonlocal elasticity theories (Thai et al., 2017). The strain gradient family includes couple stress theory, strain gradient theory, modified couple stress theory, and modified strain gradient theory. The couple stress theory (Toupin, 1962; Mindlin and Tiersten, 1962) requires two material length scale parameters because only the gradient of the rotation vector is considered. The modified couple stress theory proposed by Yang et al. (2002) reduces the number of length scale parameters from two to one by introducing an equilibrium condition of moments of couples to enforce the couple stress tensor to be symmetric.

The size effect of the microbeam can be considered by using the couple stress theory, based on which a large number of beam models have been proposed. To study the bending stiffness, Park and Gao (2006) first established a Euler-Bernoulli beam theory (EBT) model using the modified couple stress theory and the principle of minimum potential energy, and found the bending stiffness increases as the beam thickness decreases. However, the transverse shear deformation is ignored in the EBT; this fact may lead to imprecise estimates for a thick beam, where the transverse shear deformation is considerable. By taking into account shear deformation and rotational bending effects (Salvetat et al., 1999), some microscale Timoshenko beam theory (TBT) models have been developed (Wang et al., 2006, 2010). For example, Ma et al. (2008) developed a modified couple stress TBT model to study static bending and found that Poisson's effect is of great significance to beam deflection and rotation. Asghari et al. (2011) obtained the general form of the boundary conditions, as well as the closed-form analytical solutions of axial deformation, bending deflection, and cross-sectional rotation angle of a Timoshenko beam. Subsequently, the applications of the modified couple stress EBT and TBT models were extended to the bilayer, three-layered (Awrejcewicz et al., 2017), and laminated composite (Wanji et al., 2012; Chen et al., 2011b; Chen and Li, 2013; Mohammad Abadi and Daneshmehr, 2014) microbeams. Besides, the modified couple stress EBT model (Krysko et al., 2017; Xia et al., 2010; Wang et al., 2015) and TBT model (Asghari et al., 2010a) were extended to nonlinear bending by considering geometric and physical nonlinearities. Furthermore, the thermal and electrostatic effects on static bending were considered. For instance, the bending behavior of single layer (Wang et al., 2015) and bilayer (Rahaeifard, 2016) Euler-Bernoulli microbeams due to temperature rise was investigated. The static pull-in behavior of a single layer (Kong, 2013; Rahaeifard et al., 2011) and bilayer (Mojahedi and Rahaeifard, 2015) Euler-Bernoulli microbeams under static electricity action was analyzed. The results show that the size dependence has an important influence on the bending deformation of beams with thickness in the order of equivalent length scale.

Moreover, the dynamic behaviors of microbeams are also size dependent, and several studies have investigated this issue based on the modified couple stress theory. Kong et al. (2008) developed a dynamic EBT model using Hamilton's principle and found the size effect on the beam's natural frequency under different boundary conditions. Santos and Reddy (Dos Santos and Reddy, 2012) incorporated Poisson's effect and proposed a dynamic TBT model. Liu et al. (Li et al., 2019a, 2019b) established a modified couple stress-based Euler-Bernoulli beam model incorporating geometric and inertial nonlinearities, and demonstrated the size-dependency in the nonlinear regime. Besides, the thermal and electrostatic effects on free vibration were considered (Ghadiri et al., 2016; Taati et al., 2014; Ke et al., 2011; Rahaeifard et al., 2015). For instance, Ross et al. (2005) studied the vibrations of thermally activated bilayer microbeams with both ends fixed, and found the non-monotonicity of vibration frequency versus beam temperature. Ghadiri et al. (2016) proposed the modified couple stress EBT and TBT thermally induced vibration models of composite laminated microbeams, and indicated that the existence of couple stress increased the natural frequency of the beam. Ke et al. (Ke and Wang, 2012; Ke et al., 2012a) combined Timoshenko beam theory and presented the size-dependent nonlinear vibration analysis of piezoelectric nanobeams. Also, they developed a Mindlin microplate model based on the modified couple stress theory for the free vibration analysis of microplates (Ke et al., 2012b). By considering an internal material length, they discovered that the size effect is significant when the thickness of the microplate approaches the material length scale.

Although a large number of high-order continuum theories have been proposed to study the static and dynamic behaviors of the micro-/nanobeams, there are few studies on bilayer microbeams under thermal loads. Moreover, microbeams with L/h smaller than 20 often appear in MEMS-based actuators or stages (Zhou et al., 2020). For these beams, shear effects cannot be neglected (Wang, 2013; Salvetat et al., 1999). The main purpose of this work is to investigate the size and shear effects on the thermal bending of bilayer microbeams based on the TBT and modified couple stress theories. The rest of the paper is organized as follows. In Section 2, the modified couple stress theory was reviewed for clarity. In Section 3, considering the modified couple stress, we derived the strain energy of the bilayer Timoshenko beam theory. By using the principle of minimum potential energy, we obtained the higher-order governing equations and boundary conditions considering the effect of internal material length. In Section 4, taking the bilayer beam made of aluminum and polysilicon as an example, we presented the effect of beam size on the deflection. Finally, the conclusions were summarized in Section 5.

2. Modified couple stress theory

For an isotropic material, the components of the strain and stress tensors can be expressed as

$$\varepsilon_{ij} = \frac{1}{2}\left(\partial_i u_j + \partial_j u_i\right) \tag{1}$$

$$\sigma_{ij} = \lambda tr\left(\varepsilon_{ij}\right)\delta_{ij} + 2\mu\varepsilon_{ij} \tag{2}$$

where u_i and u_j are displacement components, in which $i, j = x, y, z$ for Cartesian coordinate, and λ and μ are Lame's constants, which can be obtained from

$$\lambda = \frac{E\nu}{(1+\nu)(1-2\nu)}, \mu = \frac{E}{2(1+\nu)} \tag{3}$$

where E is Young's modulus and ν is Poisson's ratio. According to the modified couple stress theory (Yang et al., 2002), the symmetric curvature tensor and deviatoric part of the couple stress tensor can be expressed as

$$\chi_{ij} = \frac{1}{2}\left(\partial_i \theta_j + \partial_j \theta_i\right) \tag{4}$$

$$m_{ij} = 2\mu l^2 \chi_{ij} \tag{5}$$

where rotation vector θ_i is related to displacement vector u_k, which has a value of

$$\theta_i = \frac{1}{2} E_{ijk}\partial_j u_k \tag{6}$$

and l denotes the material length scale parameter, which can be

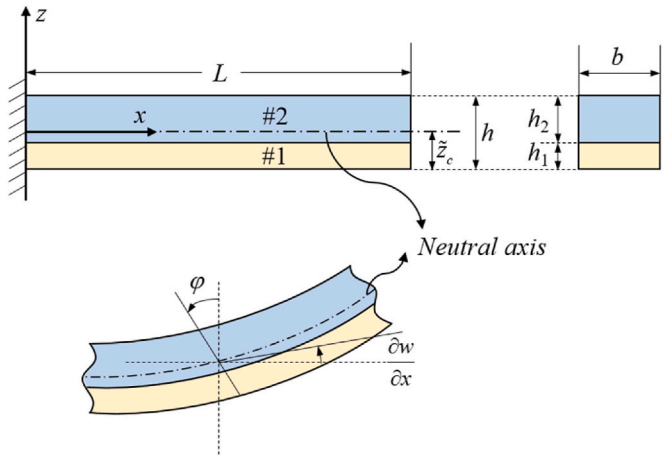

Fig. 1. Bilayer beam configuration and coordinate system.

determined from torsion tests (Yang et al., 2002) of slim cylinders with different diameters, bending (Park and Gao, 2006), and vibration (Li et al., 2018) tests of thin beams with different thicknesses.

3. Modeling bilayer beam based on the modified couple stress theory

Consider a bilayer microbeam with dimensions of length L, width b, and height h, as shown in Fig. 1. The microbeam is made of two different materials (#1 and #2) with heights of h_1 and h_2 noted that $h_1+h_2 = h$. The beam is initially in a stress-free state and is subjected to a uniform temperature rise $\triangle T$. Moreover, the position of the beam neutral axis $\tilde{z}_c$ can be obtained from the equilibrium equation along the x-axis as $\int_A \sigma_{xx} dA = 0$, where σ_{xx} is the axial normal stress component and A is the cross-sectional area of the beam (Mojahedi and Rahaeifard, 2015; Asghari et al., 2010b).

3.1. Assumptions. The present study is carried out based on the following assumptions

- The bilayer beam bends around a single axis (neutral axis), and undergoes axial and bending deformations.
- Deformation occurs in the range of linear elasticity.
- No slippage happens at the interface of the two layers.
- Constant material properties and uniform temperature throughout each layer.

3.2. Basic equations. According to TBT, the displacement components along the x, y, and z directions can be expressed as[27]

$$\begin{aligned} u_x(x,y,z) &= u(x) - z\varphi(x) \\ u_y(x,y,z) &= 0 \\ u_z(x,y,z) &= w(x) \end{aligned} \tag{7}$$

where $u(x)$ and $w(x)$ represent the axial displacement and the lateral deflection of the point $(x, 0, 0)$ on the neutral axis (x-axis), and $\varphi(x)$ is the cross-sectional rotation angle to the z-axis (Fig. 1). For thermal bending, the axial displacement $u(x)$ consists of two parts: the thermal part $u^t(x)$ and the mechanical part $u^m(x)$, i.e., $u(x) = u^t(x)+u^m(x)$. Since the axial mechanical displacement can be neglected, i.e., $u^m(x) = 0$, $u(x) = u^t(x)$. The parameter z represents the distance of a point from the neutral axis. After substituting Eq. (7) into Eq. (1), the non-zero strain components can be obtained as

$$\begin{aligned} (\varepsilon_{xx})_{1/2} &= \frac{\partial u^t}{\partial x} - z\frac{\partial \varphi}{\partial x} \\ (\varepsilon_{xz})_{1/2} &= \frac{1}{2}\left(-\varphi + \frac{\partial w}{\partial x}\right) \end{aligned} \tag{8}$$

where the subscript 1/2 (i.e., 1 or 2) denotes the value of the corresponding parameter in layer 1 or 2. When the temperature changes, the axial strain $(\varepsilon_{xx})_{1/2}$ consists of two parts: the thermal part $(\varepsilon^t_{xx})_{1/2} = \alpha_{1/2}\Delta T$, and the mechanical part as follows

$$\left(\varepsilon^m_{xx}\right)_{1/2} = \frac{\partial u^t}{\partial x} - z\frac{\partial \varphi}{\partial x} - \alpha_{1/2}\Delta T \tag{9}$$

where α is the thermal expansion coefficient and ΔT is the temperature rise. Furthermore, substituting Eqs. (8) and (9) into Eq. (2) give non-zero stress components as

$$\begin{aligned} (\sigma_{xx})_{1/2} &= \left(\lambda_{1/2} + 2\mu_{1/2}\right)\left(\frac{\partial u^t}{\partial x} - z\frac{\partial \varphi}{\partial x} - \alpha_{1/2}\Delta T\right) \\ \left(\sigma_{yy}\right)_{1/2} &= (\sigma_{zz})_{1/2} = \lambda_{1/2}\left(\frac{\partial u^t}{\partial x} - z\frac{\partial \varphi}{\partial x}\right) \\ (\sigma_{xz})_{1/2} &= 2\mu_{1/2}\varepsilon_{xz} = \mu_{1/2}\left(-\varphi + \frac{\partial w}{\partial x}\right) \end{aligned} \tag{10}$$

Substituting Eq. (7) into Eqs. (4)–(6) gives non-zero rotation, symmetric curvature, and deviatoric part of couple stress components as

$$\begin{aligned} \left(\theta_y\right)_{1/2} &= -\frac{1}{2}\left(\varphi + \frac{\partial w}{\partial x}\right) \\ \left(\chi_{xy}\right)_{1/2} &= -\frac{1}{4}\left(\frac{\partial \varphi}{\partial x} + \frac{\partial^2 w}{\partial x^2}\right) \\ \left(m_{xy}\right)_{1/2} &= -\frac{1}{2}\mu_{1/2}{l_{1/2}}^2\left(\frac{\partial \varphi}{\partial x} + \frac{\partial^2 w}{\partial x^2}\right) \end{aligned} \tag{11}$$

Additionally, the normal bending moment M, couple moment Y, and transverse shear force Q can be expressed as follows

$$\begin{aligned} M(x) &= \int_A \sigma_{xx} z dA \\ &= -\frac{\partial \varphi}{\partial x}\left[D_1\left(\left(\tilde{z}_c - h_1\right)^3 - \tilde{z}_c^{\,3}\right) + D_2\left(\left(h_1 - \tilde{z}_c\right)^3 - \left(h - \tilde{z}_c\right)^3\right)\right] b \\ &+ \frac{3}{2}\left[D_1 h_1 \alpha_1 (h_1 - 2\tilde{z}_c) + D_2 h_2 \alpha_2 (h + h_1 - 2\tilde{z}_c)\right] b\Delta T \\ Q(x) &= \int_A \sigma_{xz} dA = b(\mu_1 h_1 + \mu_2 h_2)\left(-\varphi + \frac{\partial w}{\partial x}\right) \\ Y(x) &= \int_A m_{xy} dA = -\frac{1}{2} b\left(\mu_1 h_1 l_1^2 + \mu_2 h_2 l_2^2\right)\left(\frac{\partial \varphi}{\partial x} + \frac{\partial^2 w}{\partial x^2}\right) \end{aligned} \tag{12}$$

where the coefficients related to Lame's constants are recorded as $D_1 = -(\lambda_1 + 2\mu_1)/3$, $D_2 = -(\lambda_2 + 2\mu_2)/3$.

Basing on Eqs. 8–11, the strain energy Π_s of a deformed bilayer Timoshenko beam in isotropic linear elastic materials can be obtained as

$$\Pi_s=\frac{1}{2}\int_0^L\int_A\left(\sigma_{ij}\varepsilon_{ij}+m_{ij}\chi_{ij}\right)dAdx$$
$$=\frac{1}{2}\int_0^L\left(\begin{array}{l}\int_{A_1}\left((\sigma_{xx})_1\left(\varepsilon_{xx}^m\right)_1+2(\sigma_{xz})_1(\varepsilon_{xz})_1+2\left(m_{xy}\right)_1\left(\chi_{xy}\right)_1\right)dA\\+\int_{A_2}\left((\sigma_{xx})_2\left(\varepsilon_{xx}^m\right)_2+2(\sigma_{xz})_2(\varepsilon_{xz})_2+2\left(m_{xy}\right)_2\left(\chi_{xy}\right)_2\right)dA\end{array}\right)dAdx$$
$$=\frac{1}{2}\int_0^L\left(\begin{array}{l}D_1b\dfrac{\left(\dfrac{\partial u^t}{\partial x}-(h_1-\widetilde{z}_c)\dfrac{\partial\varphi}{\partial x}-\alpha_1\Delta T\right)^3-\left(\dfrac{\partial u^t}{\partial x}+\widetilde{z}_c\dfrac{\partial\varphi}{\partial x}-\alpha_1\Delta T\right)^3}{\dfrac{\partial\varphi}{\partial x}}\\+D_2b\dfrac{\left(\dfrac{\partial u^t}{\partial x}-(h-\widetilde{z}_c)\dfrac{\partial\varphi}{\partial x}-\alpha_2\Delta T\right)^3-\left(\dfrac{\partial u^t}{\partial x}-(h_1-\widetilde{z}_c)\dfrac{\partial\varphi}{\partial x}-\alpha_2\Delta T\right)^3}{\dfrac{\partial\varphi}{\partial x}}\\+\left[\left(-\varphi+\dfrac{\partial w}{\partial x}\right)^2+\dfrac{1}{4}l_1{}^2\left(\dfrac{\partial\varphi}{\partial x}+\dfrac{\partial^2w}{\partial x^2}\right)^2\right]b\mu_1h_1\\+\left[\left(-\varphi+\dfrac{\partial w}{\partial x}\right)^2+\dfrac{1}{4}l_2{}^2\left(\dfrac{\partial\varphi}{\partial x}+\dfrac{\partial^2w}{\partial x^2}\right)^2\right]b\mu_2h_2\end{array}\right)dx \tag{13}$$

Satisfying the principle of minimum potential energy yields (Majdoub et al., 2008)

$$\delta\Pi_s=0 \tag{14}$$

Substituting Eq. (13) into Eq. (14) and letting the coefficients of δu, δw, and $\delta\varphi$ be equal to zero (the detail of the derivation is shown in Appendix A), gives the higher-order governing equation of the bilayer beam, as given by Eqs. 15–17.

$$K_1\frac{\partial^2\varphi}{\partial x^2}-K_2\left(\frac{\partial w}{\partial x}-\varphi\right)-K_3\left(\frac{\partial^2\varphi}{\partial x^2}+\frac{\partial^3w}{\partial x^3}\right)=0 \tag{15}$$

$$K_2\left(\frac{\partial\varphi}{\partial x}-\frac{\partial^2w}{\partial x^2}\right)+K_3\left(\frac{\partial^3\varphi}{\partial x^3}+\frac{\partial^4w}{\partial x^4}\right)=0 \tag{16}$$

$$\frac{\partial^2u^t}{\partial x^2}=0 \tag{17}$$

where K_1, K_2, and K_3 are the equivalent first, second, and third bending stiffnesses defined as

$$K_1=\left((\lambda+2\mu)\int_A z^2dA\right)_e=\left(\widetilde{z}_c{}^3-(\widetilde{z}_c-h_1)^3\right)D_1b+\left((h-\widetilde{z}_c)^3-(h_1-\widetilde{z}_c)^3\right)D_2b$$
$$K_2=(\mu A)_e=b(\mu_1h_1+\mu_2h_2)$$
$$K_3=\left(\frac{\mu Al^2}{4}\right)_e=\frac{b}{4}\left(\mu_1h_1l_1^2+\mu_2h_2l_2^2\right) \tag{18}$$

which reflects the ability of a Timoshenko microbeam to resist bending deformation. Similar to the reference (Mojahedi and Rahaeifard, 2015), the equivalent shear modulus and equivalent length scale parameter of the bilayer beam can be defined as $\mu_{eq}=(\mu_1h_1+\mu_2h_2)/h$ and $l_{eq}=\sqrt{(\mu_1h_1l_1^2+\mu_2h_2l_2^2)/(\mu_1h_1+\mu_2h_2)}$.

As shown in Eqs. 15–18, the governing equations of the Timoshenko bilayer beam contain additional material constants l_1 and l_2. In this way, the microstructural features have been coupled into the equations, which can reflect the size effect. This will be further illustrated through numerical results in Section 4. When the upper and lower layers are made of the same material, these equivalent bending stiffnesses in Eq. (18) will be reduced to ones of a single-layer beam (Ma et al., 2008).

Substituting Eq. (13) into Eq. (14) also gives the boundary conditions at the free end ($x=L$) as shown in Eqs. 19–22.

$$M(L)=0 \tag{19}$$

$$Q(L)+\frac{1}{2}\frac{\partial Y(L)}{\partial x}=0 \tag{20}$$

$$Y(L)=0 \tag{21}$$

$$\frac{\partial u^t(L)}{\partial x}(2D_1h_1+2D_2h_2)=2(D_1h_1\alpha_1+D_2h_2\alpha_2)\Delta T \tag{22}$$

where $M(L)$, $Y(L)$, and $Q(L)$ are the normal bending moment, couple moment, and transverse shear force at the free end of the beam ($x=L$). Also, the boundary conditions at the free end ($x=0$) are

$$u^t(0)=0 \tag{23}$$

$$w(0)=0 \tag{24}$$

$$\varphi(0)=0 \tag{25}$$

$$\frac{\partial w(0)}{\partial x}=0 \tag{26}$$

Introducing the nondimensional geometric dimensions and material property parameters defined by

$$\zeta=\frac{x}{L},\widehat{w}=\frac{wh}{12L^2},\widehat{u}^t=\frac{u^t}{L},\Psi=\varphi,\widehat{h}_1=\frac{h_1}{h},\widehat{h}_2=\frac{h_2}{h},\widehat{b}=\frac{b}{L},\eta=\frac{h}{L},\widehat{z}_c=\frac{\widetilde{z}_c}{h}$$
$$\widehat{\mu}_1=\frac{\mu_1}{\mu_1},\widehat{\mu}_2=\frac{\mu_2}{\mu_1},\widehat{D}_1=\frac{D_1}{D_1},\widehat{D}_2=\frac{D_2}{D_1},\widehat{l}_1=\frac{l_1}{h},\widehat{l}_2=\frac{l_2}{h} \tag{27}$$

and substituting Eq. (27) into Eq. (18), the first, second, and third dimensionless bending stiffnesses can be obtained as

$$\widehat{K}_1=\frac{K_1}{D_1h^3L}=\widehat{b}\left(\widehat{z}_c{}^3-(\widehat{z}_c-\widehat{h}_1)^3\right)+\widehat{b}\widehat{D}_2\left((1-\widehat{z}_c)^3-(\widehat{h}_1-\widehat{z}_c)^3\right)$$
$$\widehat{K}_2=\frac{K_2}{hL\mu_1}=\widehat{b}(\widehat{\mu}_1\widehat{h}_1+\widehat{\mu}_2\widehat{h}_2) \tag{28}$$
$$\widehat{K}_3=\frac{K_3}{Lh^3\mu_1}=\frac{\widehat{b}}{4}\left(\widehat{\mu}_1\widehat{h}_1\widehat{l}_1^2+\widehat{\mu}_2\widehat{h}_2\widehat{l}_2^2\right)$$

Subscribing Eqs. 27 and 28 into Eqs. 15–17, the governing equations can be expressed in a non-dimensional form as

$$\widehat{K}_2\left(\frac{\partial\Psi}{\partial\zeta}-12\frac{1}{\eta}\frac{\partial^2\widehat{w}}{\partial\zeta^2}\right)+\widehat{K}_3\left(\eta^2\frac{\partial^3\Psi}{\partial\zeta^3}+12\eta\frac{\partial^4\widehat{w}}{\partial\zeta^4}\right)=0 \tag{29}$$

$$\widehat{K}_1D_1\eta^2\frac{\partial^2\Psi}{\partial\zeta^2}-\widehat{K}_2\mu_1\left(12\frac{1}{\eta}\frac{\partial\widehat{w}}{\partial\zeta}-\Psi\right)-\widehat{K}_3\mu_1\left(\eta^2\frac{\partial^2\Psi}{\partial\zeta^2}+12\eta\frac{\partial^3\widehat{w}}{\partial\zeta^3}\right)=0 \tag{30}$$

$$\frac{\partial^2\widehat{u}^t}{\partial\zeta^2}=0 \tag{31}$$

For bilayer beams having a height much greater than the length scale parameters (i.e., $h\gg l_1,l_2$), these relationships can be reduced to those of the classical TBT. By using Eq. (27) in Eqs. 19–22, the associated nondimensional boundary conditions at the free end ($\zeta=1$) are obtained as

$$\eta\widehat{K}_{11}\frac{\partial\Psi(1)}{\partial\zeta}=\frac{3}{2}\left[\widehat{h}_1\alpha_1(2\widehat{z}_c-\widehat{h}_1)+\widehat{D}_2\widehat{h}_2\alpha_2(2\widehat{z}_c-2\widehat{h}_1-\widehat{h}_2)\right]\widehat{b}\Delta T \tag{32}$$

$$\widehat{K}_2\left(-\Psi(1)+12\frac{1}{\eta}\frac{\partial\widehat{w}(1)}{\partial\zeta}\right)=\widehat{K}_3\left(\eta^2\frac{\partial^2\Psi(1)}{\partial\zeta^2}+12\eta\frac{\partial^3\widehat{w}(1)}{\partial\zeta^3}\right) \tag{33}$$

$$\frac{\partial\Psi(1)}{\partial\zeta}+\frac{1}{\eta}\frac{\partial^2\widehat{w}(1)}{\partial\zeta^2}=0 \tag{34}$$

$$(\widehat{h}_1+\widehat{D}_2\widehat{h}_2)\frac{\partial\widehat{u}^t(1)}{\partial\zeta}=(\widehat{h}_1\alpha_1+\widehat{D}_2\widehat{h}_2\alpha_2)\Delta T \tag{35}$$

Table 1
Mechanical properties of two layers (Rahaeifard, 2016).

	Upper layer (Polysilicon)	Lower layer (Aluminum)
Elastic modulus (GPa)	150.0	70.0
Shear modulus (GPa)	60.98	26.3
Length scale parameter (μm)	0.27	0.35
Thermal expansion coefficient (/°C)	4.7×10^{-6}	2.55×10^{-5}

Regarding Eq. (27) and Eqs. 23–26, the dimensionless boundary conditions at the clamped end ($\zeta = 0$) can be expressed as

$$\widehat{u}^t(0) = 0 \tag{36}$$

$$\widehat{w}(0) = 0 \tag{37}$$

$$\Psi(0) = 0 \tag{38}$$

$$\frac{\partial \widehat{w}(0)}{\partial \zeta} = 0 \tag{39}$$

Considering the governing equation Eq. (31) with boundary conditions Eqs. (35) and (36), the dimensionless axial deformation of the bilayer beam can be obtained as

$$\widehat{u}^t(\zeta) = \frac{(\widehat{h}_1\alpha_1 + \widehat{D}_2\widehat{h}_2\alpha_2)\Delta T}{(\widehat{h}_1 + \widehat{D}_2\widehat{h}_2)}\zeta \tag{40}$$

Afterward, to obtain the deformed shape of the bilayer beam, the differential quadrature method (Liang et al., 2015) is employed to solve the governing Eqs. (29) and (30) together with the boundary conditions specified in Eqs. (32)–(34) and (37))–(39). Through numerical solutions, $\widehat{w}(\zeta)$ and $\Psi(\zeta)$ can be determined (details of the solution are shown in Appendix B).

4. Results and discussions

Consider a thermal bilayer actuator with an upper layer made of polysilicon and a lower layer made of aluminum. Their material property parameters (Rahaeifard, 2016), including elastic modulus, shear modulus, length scale parameters, and thermal expansion coefficients are listed in Table 1.

Fig. 2 shows the dimensionless lateral deflection of a 5-μm-long bilayer cantilever with constant $h_1/h = 0.5$, different ratios of beam height to equivalent length scale parameter ($h/l_{eq} = 2$–10), and different temperature rises ($\Delta T = 25$–100 °C). Herein, by combining the definition of the equivalent length scale parameter in Section 3 with the material parameters in Table 1, we can obtain $l_{eq} = 0.30$ μm. As a comparison, the classical dimensionless deflection of a bilayer cantilever with the same length L and h_1/h was also given in Fig. 2(a). Fig. 2(a) shows a significant size effect, i.e., the smaller the beam height, the smaller the lateral deflection of the beam, reflecting the greater the beam stiffness. As an example, for a beam with $h/l_{eq} = 2$, the equivalent stiffness is 2.0 times that of a classical one. While for $h/l_{eq} = 10$, the difference between the equivalent stiffness and the classical stiffness is reduced to 4.3%. In addition, we found that the size dependency on the beam lateral deflection is negligible for h/l_{eq}>20. This indicates that the solution of the present model is reducible to the classical model, which verifies the correctness of the present model. Fig. 2(b) shows that the dimensionless lateral deflection increases almost linearly with the increase in temperature rise. This phenomenon is also consistent with the classical thermal bending of bilayer beams. Without loss of generality, the temperature rise was set to 50 °C in all subsequent studies.

Fig. 3 displays the size-dependency of the dimensionless tip deflection of the microbeam for $h_1/h = 0.25$, 0.5, and 0.75, which are also

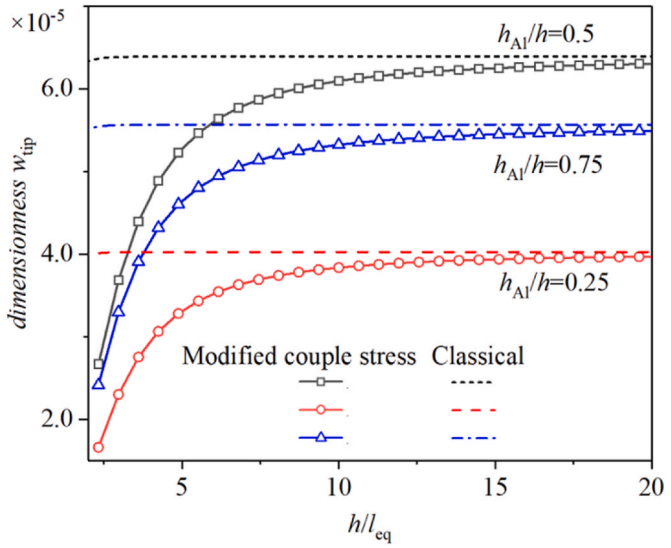

Fig. 3. Dimensionless tip deflection of the beam versus the ratio of beam height to equivalent length scale parameter ($L = 5$ μm, $\Delta T = 50$ °C).

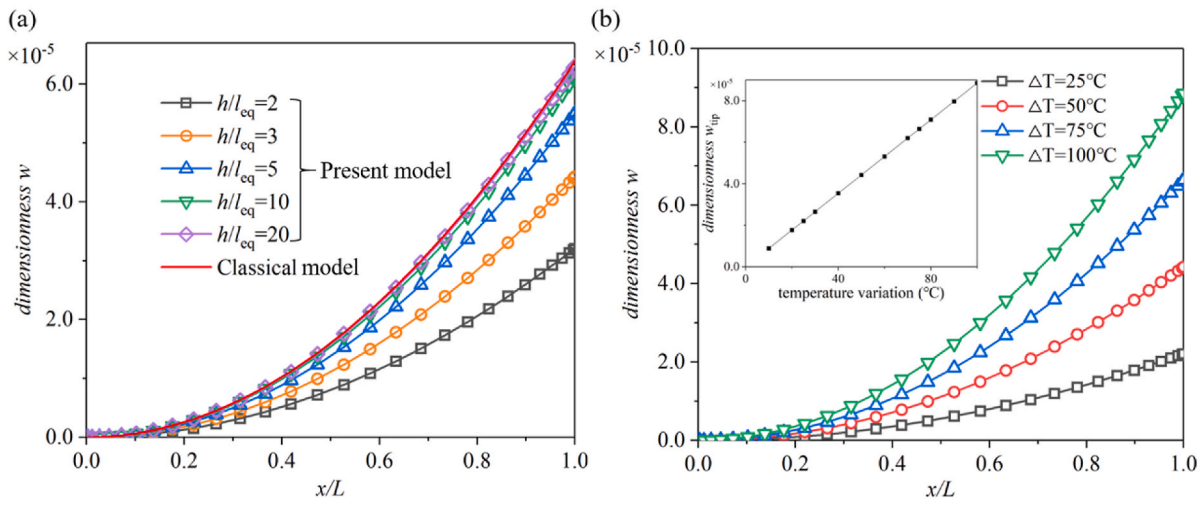

Fig. 2. Dimensionless lateral deflection of the bilayer beam. (a) $L = 5$ μm, $h_1/h = 0.5$, $\Delta T = 50$ °C. (b) $L = 5$ μm, $h_1/h = 0.5$, $h/l_{eq} = 3$.

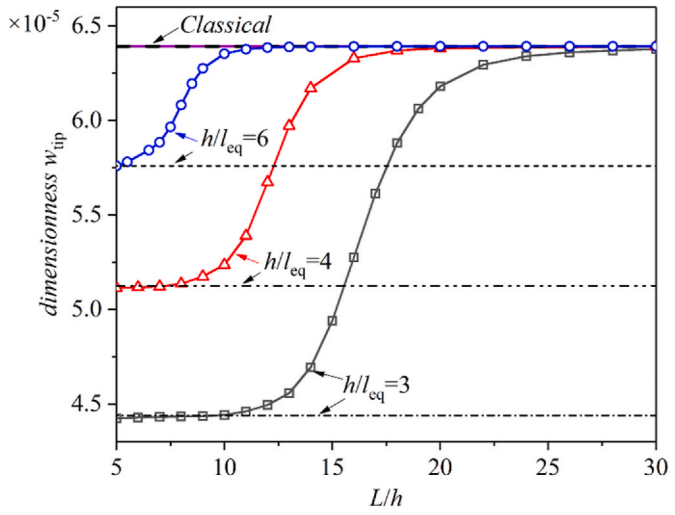

Fig. 4. Dimensionless tip deflection of the beam versus length/height ratio (ΔT = 50 °C, h_1/h = 0.5, h/l_{eq} = 3, 4, 6, ∞). Real lines represent the results of the Timoshenko beam and the dotted lines represent ones of the Euler-Bernoulli beam.

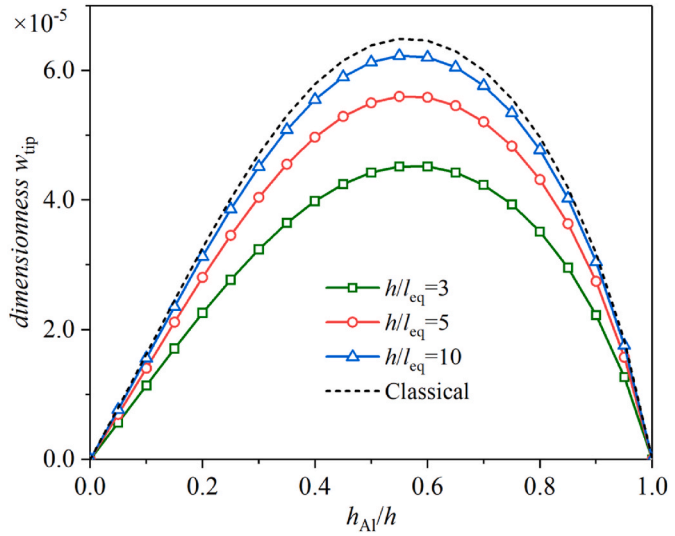

Fig. 5. Relationship between dimensionless tip deflection and height ratio (ΔT = 50 °C, L = 5 μm).

compared with their classical theoretical solutions. When $0 < h/l_{eq} < 5$, as the beam height decreases, the tip deflection of the microbeam sharply decreases, and the gap between the modified couple stress and classical theoretical solutions increases. This may be because the size effect plays an important role when the beam height is small, resulting in a significant increase in the equivalent bending stiffness of the beam. When $5 < h/l_{eq} < 15$, as the beam height increases, the tip deflection of the microbeam slowly increases and the equivalent bending stiffness slowly decreases, which indicates that the size effect is not outstanding. When $h/l_{eq} > 15$, the tip deflection of the beam tends to a stable value, which is the classical theoretical solution. Thus, the size effect can be ignored.

Fig. 4 presents the dimensionless lateral deflection of the beam tip versus length/height ratio (L/h) at h_1/h = 0.5 and h/l_{eq} = 3, 4, 6, ∞ (classical beams). For classical Timoshenko and Euler-Bernoulli beams, their dimensionless tip deflections are independent of L/h. For beams with the height of orders of the equivalent length scale parameter, the lateral deflections of both Timoshenko and Euler-Bernoulli beams are suppressed. It is worth noting that the dimensionless tip deflection of the Euler-Bernoulli beam always does not change with the variation of L/h, while that of the Timoshenko beam increases as L/h increases. E.g., for a Timoshenko beam with h/l_{eq} = 3, when L/h increases from 5 to 25, the deflection difference can reach 44.6%. Specifically, when L/h is small (corresponding to the short and stubby beam), the dimensionless tip deflection of the Timoshenko beam approaches that of the Euler-Bernoulli beam. When L/h is moderate, the dimensionless tip deflection of Timoshenko beams increases as L/h increases, and the deflection difference from the Euler-Bernoulli beam also increases. When L/h is large, the dimensionless tip deflection of Timoshenko beams converges to the classical Timoshenko solutions. The reason is that the size effect starts to work when $h/l_{eq} < 15$ (Fig. 3), which increases the equivalent bending stiffness of the beam, thus, decreases the dimensionless tip deflection of Euler-Bernoulli beams. However, for the Timoshenko beam, the size effect also increases the equivalent shear stiffness, which in turn promotes the shear deformation of the beam. Under the joint action of these two deformation mechanisms, the bilayer Timoshenko beam exhibits the characteristic that the dimensionless tip deflection is related to L/h.

Fig. 3 shows that the tip deflection of the beam is affected by the height ratio h_1/h. Thus, the relationship between the tip deflection and the height ratio was studied here, as shown in Fig. 5. The results show that the maximum deflection always occurred at $h_1/h \approx 0.55$–0.6, regardless of whether the size effect is considered or not. We infer that this phenomenon depends only on the differences in material and structural parameters between the upper and lower layers, i.e., the elasticity modulus and thickness. In addition, the equivalent stiffness of the beam increases after considering the size effects, reducing the amplitude of the maximum deflection.

5. Conclusions

This paper investigated the size-dependency of the static bending of a bilayer microbeam under thermal load. With the modified couple stress and Timoshenko beam theories, the higher-order governing equations and boundary conditions are obtained, and then solved by the differential quadrature method. The main conclusions are as follows.

(1) The analysis of a bilayer microbeam made of aluminum and polysilicon shows that the classical theory underestimates the lateral deflection of the microbeam, and the size effect on beam stiffness is significant when the beam height is on orders of the equivalent length scale parameter. For instance, for a beam with h/l_{eq} = 2, the equivalent stiffness is 2.0 times that of a classical one.

(2) Unlike the Euler-Bernoulli beam, the lateral deflection of the Timoshenko beam under temperature rise is affected by the L/h. When L/h is small, the dimensionless tip deflection $\widehat{w}_{tip}$ of the Timoshenko beam approaches that of the Euler-Bernoulli beam. When L/h is moderate, $\widehat{w}_{tip}$ of Timoshenko beam increases as L/h increases, and the deflection difference from the Euler-Bernoulli beam also increases. When L/h is large, $\widehat{w}_{tip}$ of Timoshenko beam converges to the classical Timoshenko solution.

(3) The microbeam deflection was affected by the height ratio h_1/h, and the maximum deflection always occurred at a height ratio of 0.55–0.6.

Author statement

Xuan Ye: Conceptualization, Writing – original draft, Methodology, Software, Funding acquisition; Hansong Ma: Writing- Reviewing, Investigation; Xiaoming Liu: Project administration, Supervision, Funding acquisition, Conceptualization, Writing- Reviewing and Editing, Investigation; Yueguang Wei: Project administration, Supervision,

Funding acquisition

Declaration of competing interest

The authors declare that they have no known competing financial interests or personal relationships that could have appeared to influence the work reported in this paper.

Data availability

No data was used for the research described in the article.

Acknowledgements

This work was supported by the National Natural Science Foundation of China (No. 12272203, 12022210, 12032001, 11890681, 11902311), by Youth Innovation Promotion Association CAS (2018022), and by the National Key Research Development Program of China (No. 2020-JCJQ-ZD-254).

Appendix A. The details of theoretical derivation

For this static system, the total strain energy is shown in Eq. (13), and the kinetic energy and external force work is equal to zero. Considering the principle of minimum potential energy:

$$
\begin{aligned}
\delta\Pi_s = & \int_0^L \left[-b(\mu_1 h_1 + \mu_2 h_2)\left(-\frac{\partial\varphi}{\partial x} + \frac{\partial^2 w}{\partial x^2}\right) + \frac{b}{4}\left(\mu_1 h_1 l_1^2 + \mu_2 h_2 l_2^2\right)\left(\frac{\partial^3\varphi}{\partial x^3} + \frac{\partial^4 w}{\partial x^4}\right)\right]\delta w dx \\
& + \int_0^L \left\{ \begin{array}{l}
\dfrac{1}{2}D_1 b\left[\dfrac{\partial}{\partial x}\left(\dfrac{\left(\dfrac{\partial u^t}{\partial x} - (h_1 - \widetilde{z}_c)\dfrac{\partial\varphi}{\partial x} - \alpha_1\Delta T\right)^2\left(\dfrac{\partial u^t}{\partial x} + 2(h_1 - \widetilde{z}_c)\dfrac{\partial\varphi}{\partial x} - \alpha_1\Delta T\right)}{\left(\dfrac{\partial\varphi}{\partial x}\right)^2}\right)\right. \\
\left. -\dfrac{\partial}{\partial x}\left(\dfrac{\left(\dfrac{\partial u^t}{\partial x} + \widetilde{z}_c\dfrac{\partial\varphi}{\partial x} - \alpha_1\Delta T\right)^2\left(\dfrac{\partial u^t}{\partial x} - 2\widetilde{z}_c\dfrac{\partial\varphi}{\partial x} - \alpha_1\Delta T\right)}{\left(\dfrac{\partial\varphi}{\partial x}\right)^2}\right)\right] \\
+\dfrac{1}{2}D_2 b\left[\dfrac{\partial}{\partial x}\left(\dfrac{\left(\dfrac{\partial u^t}{\partial x} - (h - \widetilde{z}_c)\dfrac{\partial\varphi}{\partial x} - \alpha_2\Delta T\right)^2\left(\dfrac{\partial u^t}{\partial x} + 2(h - \widetilde{z}_c)\dfrac{\partial\varphi}{\partial x} - \alpha_2\Delta T\right)}{\left(\dfrac{\partial\varphi}{\partial x}\right)^2}\right)\right. \\
\left. -\dfrac{\partial}{\partial x}\left(\dfrac{\left(\dfrac{\partial u^t}{\partial x} - (h_1 - \widetilde{z}_c)\dfrac{\partial\varphi}{\partial x} - \alpha_2\Delta T\right)^2\left(\dfrac{\partial u^t}{\partial x} + 2(h_1 - \widetilde{z}_c)\dfrac{\partial\varphi}{\partial x} - \alpha_2\Delta T\right)}{\left(\dfrac{\partial\varphi}{\partial x}\right)^2}\right)\right] \\
+b(\mu_1 h_1 + \mu_2 h_2)\left(\varphi - \dfrac{\partial w}{\partial x}\right) - \dfrac{b}{4}\left(\mu_1 h_1 l_1^2 + \mu_2 h_2 l_2^2\right)\left(\dfrac{\partial^2\varphi}{\partial x^2} + \dfrac{\partial^3 w}{\partial x^3}\right)
\end{array}\right\}\delta\varphi dx \\
& + \int_0^L \left\{ \begin{array}{l}
\dfrac{1}{2}D_1 b\left[-\dfrac{\partial}{\partial x}\left(\dfrac{3\left(\dfrac{\partial u^t}{\partial x} - (h_1 - \widetilde{z}_c)\dfrac{\partial\varphi}{\partial x} - \alpha_1\Delta T\right)^2}{\dfrac{\partial\varphi}{\partial x}}\right) + \dfrac{\partial}{\partial x}\left(\dfrac{3\left(\dfrac{\partial u^t}{\partial x} + \widetilde{z}_c\dfrac{\partial\varphi}{\partial x} - \alpha_1\Delta T\right)^2}{\dfrac{\partial\varphi}{\partial x}}\right)\right] \\
+\dfrac{1}{2}D_2 b\left[-\dfrac{\partial}{\partial x}\left(\dfrac{3\left(\dfrac{\partial u^t}{\partial x} - (h - \widetilde{z}_c)\dfrac{\partial\varphi}{\partial x} - \alpha_2\Delta T\right)^2}{\dfrac{\partial\varphi}{\partial x}}\right) + \dfrac{\partial}{\partial x}\left(\dfrac{3\left(\dfrac{\partial u^t}{\partial x} - (h_1 - \widetilde{z}_c)\dfrac{\partial\varphi}{\partial x} - \alpha_2\Delta T\right)^2}{\dfrac{\partial\varphi}{\partial x}}\right)\right]
\end{array}\right\}\delta u^t dx
\end{aligned}
$$

$$
\begin{aligned}
&+\left\{\begin{array}{l}
\frac{1}{2}D_1 b\left[\frac{3\left(\frac{\partial u^t}{\partial x}-(h_1-\widetilde{z}_c)\frac{\partial \varphi}{\partial x}-\alpha_1\Delta T\right)^2}{\frac{\partial \varphi}{\partial x}}-\frac{3\left(\frac{\partial u^t}{\partial x}+\widetilde{z}_c\frac{\partial \varphi}{\partial x}-\alpha_1\Delta T\right)^2}{\frac{\partial \varphi}{\partial x}}\right] \\
+\frac{1}{2}D_2 b\left[\frac{3\left(\frac{\partial u^t}{\partial x}-(h-\widetilde{z}_c)\frac{\partial \varphi}{\partial x}-\alpha_2\Delta T\right)^2}{\frac{\partial \varphi}{\partial x}}-\frac{3\left(\frac{\partial u^t}{\partial x}-(h_1-\widetilde{z}_c)\frac{\partial \varphi}{\partial x}-\alpha_2\Delta T\right)^2}{\frac{\partial \varphi}{\partial x}}\right]
\end{array}\right\}\delta u^t|_0^L \\
&+\left\{\begin{array}{l}
\frac{1}{2}D_1 b\left[\begin{array}{l}
-\frac{\left(\frac{\partial u^t}{\partial x}-(h_1-\widetilde{z}_c)\frac{\partial \varphi}{\partial x}-\alpha_1\Delta T\right)^2\left(\frac{\partial u^t}{\partial x}+2(h_1-\widetilde{z}_c)\frac{\partial \varphi}{\partial x}-\alpha_1\Delta T\right)}{\left(\frac{\partial \varphi}{\partial x}\right)^2} \\
+\frac{\left(\frac{\partial u^t}{\partial x}+\widetilde{z}_c\frac{\partial \varphi}{\partial x}-\alpha_1\Delta T\right)^2\left(\frac{\partial u^t}{\partial x}-2\widetilde{z}_c\frac{\partial \varphi}{\partial x}-\alpha_1\Delta T\right)}{\left(\frac{\partial \varphi}{\partial x}\right)^2}
\end{array}\right] \\
+\frac{1}{2}D_2 b\left[\begin{array}{l}
-\frac{\left(\frac{\partial u^t}{\partial x}-(h-\widetilde{z}_c)\frac{\partial \varphi}{\partial x}-\alpha_2\Delta T\right)^2\left(\frac{\partial u^t}{\partial x}+2(h-\widetilde{z}_c)\frac{\partial \varphi}{\partial x}-\alpha_2\Delta T\right)}{\left(\frac{\partial \varphi}{\partial x}\right)^2} \\
+\frac{\left(\frac{\partial u^t}{\partial x}-(h_1-\widetilde{z}_c)\frac{\partial \varphi}{\partial x}-\alpha_2\Delta T\right)^2\left(\frac{\partial u^t}{\partial x}+2(h_1-\widetilde{z}_c)\frac{\partial \varphi}{\partial x}-\alpha_2\Delta T\right)}{\left(\frac{\partial \varphi}{\partial x}\right)^2}
\end{array}\right] \\
+\frac{b}{4}\left(\mu_1 h_1 l_1^2+\mu_2 h_2 l_2^2\right)\left(\frac{\partial \varphi}{\partial x}+\frac{\partial^2 w}{\partial x^2}\right)
\end{array}\right\}\delta\varphi|_0^L \\
&+\left\{b(\mu_1 h_1+\mu_2 h_2)\left(-\varphi+\frac{\partial w}{\partial x}\right)-\frac{b}{4}\left(\mu_1 h_1 l_1^2+\mu_2 h_2 l_2^2\right)\left(\frac{\partial^2 \varphi}{\partial x^2}+\frac{\partial^3 w}{\partial x^3}\right)\right\}\delta w|_0^L \\
&+\frac{b}{4}\left(\mu_1 h_1 l_1^2+\mu_2 h_2 l_2^2\right)\left(\frac{\partial \varphi}{\partial x}+\frac{\partial^2 w}{\partial x^2}\right)\delta\left(\frac{\partial w}{\partial x}\right)\Big|_0^L=0
\end{aligned}
\tag{A.1}
$$

Letting the coefficients of δu, δw, and $\delta\varphi$ be equal to zero, one can obtain the governing equations as:

$$
(\mu_1 h_1+\mu_2 h_2)\left(\frac{\partial \varphi}{\partial x}-\frac{\partial^2 w}{\partial x^2}\right)+\frac{\mu_1 h_1 l_1^2+\mu_2 h_2 l_2^2}{4}\left(\frac{\partial^3 \varphi}{\partial x^3}+\frac{\partial^4 w}{\partial x^4}\right)=0 \tag{A.2}
$$

$$
\begin{aligned}
&2\left[\left(\widetilde{z}_c{}^3-(\widetilde{z}_c-h_1)^3\right)D_1 b+\left((h-\widetilde{z}_c)^3-(h_1-\widetilde{z}_c)^3\right)D_2 b-\frac{b}{4}\left(\mu_1 h_1 l_1^2+\mu_2 h_2 l_2^2\right)\right]\frac{\partial^2 \varphi}{\partial x^2} \\
&\qquad +2b(\mu_1 h_1+\mu_2 h_2)\left(\varphi-\frac{\partial w}{\partial x}\right)-\frac{b}{2}\left(\mu_1 h_1 l_1^2+\mu_2 h_2 l_2^2\right)\frac{\partial^3 w}{\partial x^3}=0
\end{aligned}
\tag{A.3}
$$

$$
2(D_1 h_1 b+D_2 h_2 b)\frac{\partial^2 u^t}{\partial x^2}=0 \tag{A.4}
$$

Considering the beam cantilever structure (with one end fixed and the other end free), one can obtain boundary conditions as follow:

$$
\begin{aligned}
&\frac{\partial \varphi(L)}{\partial x}\left[D_1\left((\widetilde{z}_c-h_1)^3-\widetilde{z}_c{}^3\right)+D_2\left((h_1-\widetilde{z}_c)^3-(h-\widetilde{z}_c)^3\right)\right] \\
&\quad=\frac{3}{2}\left[D_1 h_1\alpha_1(h_1-2\widetilde{z}_c)+D_2 h_2\alpha_2(h+h_1-2\widetilde{z}_c)\right]\Delta T
\end{aligned}
\tag{A.5}
$$

$$
(\mu_1 h_1+\mu_2 h_2)\left(-\varphi(L)+\frac{\partial w(L)}{\partial x}\right)=\frac{1}{4}\left(\mu_1 h_1 l_1^2+\mu_2 h_2 l_2^2\right)\left(\frac{\partial^2 \varphi(L)}{\partial x^2}+\frac{\partial^3 w(L)}{\partial x^3}\right) \tag{A.6}
$$

$$
\frac{\partial \varphi(L)}{\partial x}+\frac{\partial^2 w(L)}{\partial x^2}=0 \tag{A.7}
$$

$$
\frac{\partial u^t(L)}{\partial x}(D_1 h_1+D_2 h_2)=(D_1 h_1\alpha_1+D_2 h_2\alpha_2)\Delta T \tag{A.8}
$$

$$u^{t}(0)=0 \tag{A.9}$$

$$w(0)=0 \tag{A.10}$$

$$\varphi(0)=0 \tag{A.11}$$

$$\frac{\partial w(0)}{\partial x}=0 \tag{A.12}$$

Appendix B. Solution of governing equations and boundary conditions

The differential quadrature method is taken to solve the governing equations Eqs. (29) and (30) together with the boundary conditions specified in Eqs. (32)–(34) and (37)–(39) to obtain $\widehat{w}(\zeta)$ and $\Psi(\zeta)$. The dimensionless beam can be discretized as

$$\zeta_i=\frac{1}{2}\left(1-\cos\frac{\pi(i-1)}{N-1}\right)\ (i=1,2...N) \tag{B.1}$$

To solve the complex Eqs. (29) and (30), the dimensionless $\widehat{w}(\zeta)$ and $\Psi(\zeta)$ can be expressed as a linear combination of a complete set of linearly independent basis functions

$$\begin{aligned}\widehat{w}(\zeta_i)&=\sum_{j=1}^{N} l_j(\zeta_i)\widehat{w}(\zeta_j)\\ \Psi(\zeta_i)&=\sum_{j=1}^{N} l_j(\zeta_i)\Psi(\zeta_j)\end{aligned} \tag{B.2}$$

where the basis function can be Lagrange interpolation polynomials as $l_j(\zeta_i)=\prod_{\substack{k=1\\k\neq j}}^{N}\frac{\zeta_i-\zeta_k}{\zeta_j-\zeta_k}$. Thus, the higher derivatives of $\widehat{w}(\zeta)$ and $\Psi(\zeta)$ can be obtained as

$$\begin{aligned}\widehat{w}^{(n)}(\zeta_i)&=\sum_{j=1}^{N} l_j^{(n)}(\zeta_i)\widehat{w}(\zeta_j)\\ \Psi^{(n)}(\zeta_i)&=\sum_{j=1}^{N} l_j^{(n)}(\zeta_i)\Psi(\zeta_j)\ (n=1,2,3,4)\end{aligned} \tag{B.3}$$

and the higher derivatives of the basis function are

$$\begin{cases} l_j^{(1)}(\zeta_i)=A_{ij}=\begin{cases}\prod_{k=1}^{N}(\zeta_i-\zeta_k) & \\ \dfrac{\prod_{k\neq i,j}^{N}(\zeta_i-\zeta_k)}{\prod_{k=1}^{N}(\zeta_j-\zeta_k)}\ (i\neq j) & \\ \sum_{\substack{k=1\\k\neq i}}^{N}\dfrac{1}{\zeta_i-\zeta_k}(i=j) & \end{cases}\\ l_j^{(2)}(\zeta_i)=B_{ij}=\sum_{k=1}^{N}A_{ik}A_{kj}\ (i,j=1,2...N)\\ l_j^{(3)}(\zeta_i)=C_{ij}=\sum_{k=1}^{N}A_{ik}B_{kj}=\sum_{k=1}^{N}B_{ik}A_{kj}\\ l_j^{(4)}(\zeta_i)=D_{ij}=\sum_{k=1}^{N}A_{ik}C_{kj}=\sum_{k=1}^{N}B_{ik}B_{kj}=\sum_{k=1}^{N}C_{ik}A_{kj}\end{cases} \tag{B.4}$$

Moreover, governing equations from Eqs. (29) and (30) and boundary conditions from Eqs. (32)–(34) and (37)–(39) can be discretized as

$$
\begin{aligned}
&\left(\widehat{K}_2 A_{ij} + \eta^2 \widehat{K}_3 C_{ij}\right)\Psi_j + \left(\eta^3 \widehat{K}_3 D_{ij} - \eta\, \widehat{K}_2 B_{ij}\right)\widehat{w}_j = 0 \\
&\left(\eta^2 \widehat{K}_1 D_1 B_{ij} + \mu_1 \widehat{K}_2 L_{ij} - \mu_1 \eta^2 \widehat{K}_3 B_{ij}\right)\Psi_j - \left(\eta\mu_1 \widehat{K}_2 A_{ij} + \eta^3 \mu_1 \widehat{K}_3 C_{ij}\right)\widehat{w}_j = 0 \\
&at\ \zeta = \zeta_N = 1 (i = N)\ , \\
&\quad \eta \widehat{K}_1 A_{ij}\Psi_j = \frac{3}{2}[\widehat{h}_1 \alpha_1 (2\widehat{z}_c - \widehat{h}_1) + \widehat{D}_2 \widehat{h}_2 \alpha_2 (2\widehat{z}_c - 2\widehat{h}_1 - \widehat{h}_2)]\widehat{b}\Delta T \\
&\quad -\left(\eta^2 \widehat{K}_3 B_{ij} + \widehat{K}_2 L_{ij}\right)\Psi_j + \left(\eta \widehat{K}_2 A_{ij} - \eta^3 \widehat{K}_3 C_{ij}\right)\widehat{w}_j = 0 \\
&A_{ij}\Psi_j + \eta B_{ij}\widehat{w}_j = 0 \\
&at\ \zeta = \zeta_1 = 0 (i = 1)\ , \\
&\widehat{w}(\zeta_1) = 0 \\
&\Psi(\zeta_1) = 0 \\
&A_{ij}\widehat{w}_j = 0
\end{aligned}
\tag{B.5}
$$

To sum up, $\widehat{w}_j$ and Ψ_j ($j = 1,2 \ldots N$) can be obtained to calculate the static deflection.

References

Akgöz, B., Civalek, Ö., 2011. Strain gradient elasticity and modified couple stress models for buckling analysis of axially loaded micro-scaled beams. Int. J. Eng. Sci. 49, 1268–1280.

Akgöz, B., Civalek, Ö., 2013. A size-dependent shear deformation beam model based on the strain gradient elasticity theory. Int. J. Eng. Sci. 70, 1–14.

Asghari, M., Kahrobaiyan, M.H., Ahmadian, M.T., 2010a. A nonlinear Timoshenko beam formulation based on the modified couple stress theory. Int. J. Eng. Sci. 48, 1749–1761.

Asghari, M., Ahmadian, M.T., Kahrobaiyan, M.H., Rahaeifard, M., 2010b. On the size-dependent behavior of functionally graded micro-beams. Mater. Des. 31, 2324–2329, 1980-2015.

Asghari, M., Kahrobaiyan, M.H., Rahaeifard, M., Ahmadian, M.T., 2011. Investigation of the size effects in Timoshenko beams based on the couple stress theory. Arch. Appl. Mech. 81, 863–874.

Awrejcewicz, J., Krysko, V.A., Pavlov, S.P., Zhigalov, M.V., Krysko, A.V., 2017. Mathematical model of a three-layer micro- and nano-beams based on the hypotheses of the Grigolyuk–Chulkov and the modified couple stress theory. Int. J. Solid Struct. 117, 39–50.

Chen, W.J., Li, X.P., 2013. Size-dependent free vibration analysis of composite laminated Timoshenko beam based on new modified couple stress theory. Arch. Appl. Mech. 83, 431–444.

Chen, L., et al., 2011a. High-performance, low-voltage, and easy-operable bending actuator based on aligned carbon nanotube/polymer composites. ACS Nano 5, 1588–1593.

Chen, W., Li, L., Xu, M., 2011b. A modified couple stress model for bending analysis of composite laminated beams with first order shear deformation. Compos. Struct. 93, 2723–2732.

Cheng, W., Hu, G., 2021. Odd elasticity realized by piezoelectric material with linear feedback. Sci. China Phys. Mech. Astron. 64, 2.

Cheng, H., Yang, H., Li, X., Wang, Y., 2013. Field-effect piezoresistors for vibration detection of nanobeams by using monolithically integrated MOS capacitors. J. Micromech. Microeng. 23, 025011.

Dai, H.L., Wang, Y.K., Wang, L., 2015. Nonlinear dynamics of cantilevered microbeams based on modified couple stress theory. Int. J. Eng. Sci. 94, 103–112.

Dos Santos, J.V.A., Reddy, J.N., 2012. Free vibration and buckling analysis of beams with a modified couple-stress theory. Int. J. Appl. Mechanics 4, 1250026.

Ghadiri, M., Zajkani, A., Akbarizadeh, M.R., 2016. Thermal effect on dynamics of thin and thick composite laminated microbeams by modified couple stress theory for different boundary conditions. Appl. Phys. A 122, 1023.

Hao, N., Ke, L.-L., 2022. Softening-spring phenomenon in large amplitude vibration of two-layer bi-material beams. Int. J. Struct. Stabil. Dynam. 22, 2250106.

Hao, N., Zhu, L., Wu, Z., Ke, L., 2023. Softening-spring nonlinearity in large amplitude vibration of unsymmetric double-layer lattice truss core sandwich beams. Thin-Walled Struct. 182, 110164.

Ke, L.-L., Wang, Y.-S., 2012. Thermoelectric-mechanical vibration of piezoelectric nanobeams based on the nonlocal theory. Smart Mater. Struct. 21, 025018.

Ke, L.-L., Wang, Y.-S., Wang, Z.-D., 2011. Thermal effect on free vibration and buckling of size-dependent microbeams. Phys. E Low-dimens. Syst. Nanostruct. 43, 1387–1393.

Ke, L.-L., Wang, Y.-S., Wang, Z.-D., 2012a. Nonlinear vibration of the piezoelectric nanobeams based on the nonlocal theory. Compos. Struct. 94, 2038–2047.

Ke, L.-L., Wang, Y.-S., Yang, J., Kitipornchai, S., 2012b. Free vibration of size-dependent Mindlin microplates based on the modified couple stress theory. J. Sound Vib. 331, 94–106.

Kim, Y.-S., Shi, H., Dagalakis, N.G., Gupta, S.K., 2016. Design of a MEMS-based motion stage based on a lever mechanism for generating large displacements and forces. J. Micromech. Microeng. 26, 095008.

Kong, S., 2013. Size effect on pull-in behavior of electrostatically actuated microbeams based on a modified couple stress theory. Appl. Math. Model. 37, 7481–7488.

Kong, S., Zhou, S., Nie, Z., Wang, K., 2008. The size-dependent natural frequency of Bernoulli–Euler micro-beams. Int. J. Eng. Sci. 46, 427–437.

Krysko, A.V., Awrejcewicz, J., Zhigalov, M.V., Pavlov, S.P., Krysko, V.A., 2017. Nonlinear behaviour of different flexible size-dependent beams models based on the modified couple stress theory. Part 1: governing equations and static analysis of flexible beams. Int. J. Non Lin. Mech. 93, 96–105.

Lam, D.C.C., Yang, F., Chong, A.C.M., Wang, J., Tong, P., 2003. Experiments and theory in strain gradient elasticity. J. Mech. Phys. Solid. 51, 1477–1508.

Leeladhar, Raturi, P., Kumar, A., Singh, J.P., 2017. Graphene-polydimethylsiloxane/chromium bilayer-based flexible, reversible, and large bendable photomechanical actuators. Smart Mater. Struct. 26, 095030.

Li, Z., et al., 2018. A standard experimental method for determining the material length scale based on modified couple stress theory. Int. J. Mech. Sci. 141, 198–205.

Li, Z., et al., 2019a. Experimental investigation and theoretical modelling on nonlinear dynamics of cantilevered microbeams. Eur. J. Mech. Solid. 78, 103834.

Li, Z., et al., 2019b. Experimental investigation on size-dependent higher-mode vibration of cantilever microbeams. Microsyst. Technol. 25, 3005–3015.

Liang, L.-N., Ke, L.-L., Wang, Y.-S., Yang, J., Kitipornchai, S., 2015. Flexural vibration of an atomic force microscope cantilever based on modified couple stress theory. Int. J. Struct. Stabil. Dynam. 15, 1540025.

Ma, H.M., Gao, X.-L., Reddy, J.N., 2008. A microstructure-dependent Timoshenko beam model based on a modified couple stress theory. J. Mech. Phys. Solid. 56, 3379–3391.

Majdoub, M.S., Sharma, P., Cagin, T., 2008. Enhanced size-dependent piezoelectricity and elasticity in nanostructures due to the flexoelectric effect. Phys. Rev. B 77, 125424.

Mindlin, R.D., Tiersten, H.F., 1962. Effects of couple-stresses in linear elasticity. Arch. Ration. Mech. Anal. 11, 415–448.

Mohammad Abadi, M., Daneshmehr, A.R., 2014. An investigation of modified couple stress theory in buckling analysis of micro composite laminated Euler–Bernoulli and Timoshenko beams. Int. J. Eng. Sci. 75, 40–53.

Mojahedi, M., Rahaeifard, M., 2015. Static deflection and pull-In instability of the electrostatically actuated bilayer microcantilever beams. Int. J. Appl. Mechanics 7, 1550090.

Park, S.K., Gao, X.-L., 2006. Bernoulli–Euler beam model based on a modified couple stress theory. J. Micromech. Microeng. 16, 2355.

Potekhina, A., Wang, C., 2019. Review of electrothermal actuators and applications. Actuators 8, 69.

Rahaeifard, M., 2016. Static behavior of bilayer microcantilevers under thermal actuation. Int. J. Eng. Sci. 107, 28–35.

Rahaeifard, M., Kahrobaiyan, M.H., Asghari, M., Ahmadian, M.T., 2011. Static pull-in analysis of microcantilevers based on the modified couple stress theory. Sensor Actuator Phys. 171, 370–374.

Rahaeifard, M., Ahmadian, M.T., Firoozbakhsh, K., 2015. Vibration analysis of electrostatically actuated nonlinear microbridges based on the modified couple stress theory. Appl. Math. Model. 39, 6694–6704.

Ross, D.S., Cabal, A., Trauernicht, D., Lebens, J., 2005. Temperature-dependent vibrations of bilayer microbeams. Sensor Actuator Phys. 119, 537–543.

Sachyani, E., et al., 2017. Enhanced movement of CNT-based actuators by a three-Layered structure with controlled resistivity. Sensor. Actuator. B Chem. 252, 1071–1077.

Salvetat, J.-P., et al., 1999. Elastic and shear moduli of single-walled carbon nanotube ropes. Phys. Rev. Lett. 82, 944–947.

Sellinger, A.T., Wang, D.H., Tan, L.-S., Vaia, R.A., 2010. Electrothermal polymer nanocomposite actuators. Adv. Mater. 22, 3430–3435.

Stölken, J.S., Evans, A.G., 1998. A microbend test method for measuring the plasticity length scale. Acta Mater. 46, 5109–5115.

Taati, E., Molaei Najafabadi, M., Basirat Tabrizi, H., 2014. Size-dependent generalized thermoelasticity model for Timoshenko microbeams. Acta Mech. 225, 1823–1842.

Thai, H.-T., Vo, T.P., Nguyen, T.-K., Kim, S.-E., 2017. A review of continuum mechanics models for size-dependent analysis of beams and plates. Compos. Struct. 177, 196–219.

Toupin, R.A., 1962. Elastic materials with couple-stresses. Arch. Ration. Mech. Anal. 11, 385–414.
Wang, G., 2013. Analysis of bimorph piezoelectric beam energy harvesters using Timoshenko and Euler–Bernoulli beam theory. J. Intell. Mater. Syst. Struct. 24, 226–239.
Wang, C.M., Zhang, Y.Y., Ramesh, S.S., Kitipornchai, S., 2006. Buckling analysis of micro- and nano-rods/tubes based on nonlocal Timoshenko beam theory. J. Phys. D Appl. Phys. 39, 3904.
Wang, B., Zhao, J., Zhou, S., 2010. A micro scale Timoshenko beam model based on strain gradient elasticity theory. Eur. J. Mech. Solid. 29, 591–599.
Wang, Y.-G., Lin, W.-H., Liu, N., 2015. Nonlinear bending and post-buckling of extensible microscale beams based on modified couple stress theory. Appl. Math. Model. 39, 117–127.
Wang, C., et al., 2016. A solution-processed high-temperature, flexible, thin-film actuator. Adv. Mater. 28, 8618–8624.
Wang, T., et al., 2020. A phase-field model of thermo-elastic coupled brittle fracture with explicit time integration. Comput. Mech. 65, 1305–1321.
Wanji, C., Chen, W., Sze, K.Y., 2012. A model of composite laminated Reddy beam based on a modified couple-stress theory. Compos. Struct. 94, 2599–2609.
Xia, W., Wang, L., Yin, L., 2010. Nonlinear non-classical microscale beams: static bending, postbuckling and free vibration. Int. J. Eng. Sci. 48, 2044–2053.
Yang, F., Chong, A.C.M., Lam, D.C.C., Tong, P., 2002. Couple stress based strain gradient theory for elasticity. Int. J. Solid Struct. 39, 2731–2743.
Zhou, G., Lim, Z.H., Qi, Y., Zhou, G., 2020. Single-pixel MEMS imaging systems. Micromachines 11, 219.